Journal of Materials Chemistry C

Accepted Manuscript

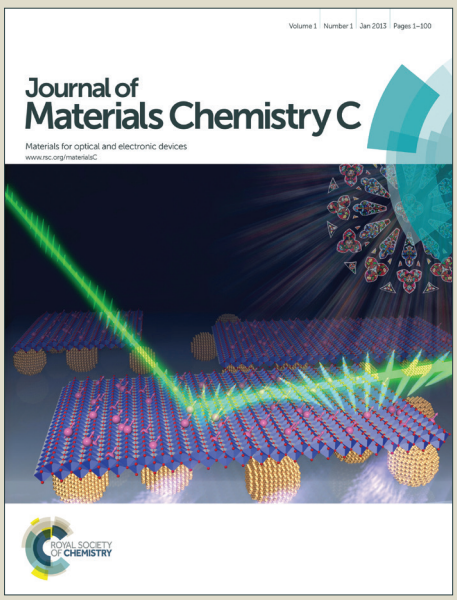

ROYAL SOCIETY OF CHEMISTRY

www.rsc.org/materialsC

Journal of Materials Chemistry C

ARTICLE

Indene-1,3-dionemethylene-4*H*-pyran derivatives containing alkoxy chains of various lengths: Aggregation-induced emission enhancement, mechanofluorochromic properties and solvent-induced emission changes

Received 00th January 20xx,
Accepted 00th January 20xx

DOI: 10.1039/x0xx00000x

www.rsc.org/

Yanze Liu,[a] Yunxiang Lei,[a] Fei Li,[b] Jiuxi Chen,[a] Miaochang Liu,[a] Xiaobo Huang,[*a] Wenxia Gao,[a] Huayue Wu,[*a] Jinchang Ding[a] and Yixiang Cheng[*b]

A series of D-π-A indene-1,3-dionemethylene-4*H*-pyran (IDMP) derivatives with aggregation-induced emission enhancement phenomena were synthesized using indene-1,3-dionemethylene as an electron acceptor and a phenyl ring containing different lengths of alkoxy chains as an electron donor. The as-synthesized IDMP solids emit from red to yellow fluorescence and the fluorescence emissions show obvious blue shifts with the increase of the length of the alkoxy chains. Some of these compounds exhibit obvious redshift mechanofluorochromic (MFC) properties, and the longer the alkoxy chain, the more remarkable the MFC properties. Moreover, the fluorescence emission of these compounds can be switched by using various external stimuli such as grinding, annealing, and solvent fuming. In particular, solvent-induced emission changes similar to those resulting from MFC properties can be achieved by a simple dissolution–desolvation process in different solvent systems, such as chloroform and THF. X-ray diffraction experiments reveal that the MFC properties and solvent-induced emission changes can both be considered as altered-morphology-induced emission properties, which are ascribed to the transformation between crystalline and amorphous states. The results indicate that the subtle manipulation of the length of the alkoxy chain of IDMP derivatives could endow them with unique and tunable solid-state optical properties.

Introduction

In the past 10 years, organic materials exhibiting reversible solid-state fluorescence changes induced by external stimuli, especially mechanofluorochromic (MFC) materials,[1] have attracted much interest owing to their promising applications as fluorescent sensors,[2] data storage,[3] and security inks,[4] etc. Generally, solid-state fluorescence changes can be achieved by either a chemical or physical structural change. Compared with chemical alteration of the molecular structures, changing the molecular packing mode is believed to be an easier way to achieve the dynamic control of highly efficient and reversible solid-state fluorescence.[1a] In 2001 and 2002, Tang *et al.*[5] and Park *et al.*[6] reported some aggregation-induced emission (AIE) and aggregation-induced emission enhancement (AIEE) molecules in the aggregate state, respectively. These are contrary to many conventional fluorescent materials where aggregation-caused quenching (ACQ) results from strong intermolecular π–π stacking interactions and nonradiative decay. Many AIE/AIEE-active compounds have highly twisted conformations that can hinder intermolecular close stacking and intense π–π interaction, which is an advantage and allows the change of molecular packing mode in the solid state upon exposure to external stimuli.[7] In 2010, Park *et al.*[8] reported the first molecule, named α,α'-dicyano-1,4-bis(4-butoxystyryl)benzene, with both AIE activity and MFC property. Since then, many AIE/AIEE-active organic compounds with MFC activity have been reported, such as cyano-substituted diarylethenes,[9] diphenyldibenzofulvenes,[10] tetraphenylethenes,[11] and 9,10-divinylanthracenes,[7,12] etc. To date, MFC compounds are still at the initial stages of development and only a small number have been reported. Most of them emit from blue to yellow fluorescence, as both original solids and ground solids, while solids that emit red fluorescence are relatively rare.[11f,12a–e,13] A common way to widen the range of the emission colours of fluorescent compounds is to construct a donor-π-acceptor (D-π-A) structure, which leads to a greater redshift emission *via* intramolecular charge transfer (ICT).[14] Additionally, some studies have suggested that D-π-A emitters with AIE/AIEE-activity always contribute to the realization of fluorescence change under pressure.[15] Therefore, the development of novel D-π-A MFC materials emitting orange–red solid-state fluorescence is a very attractive topic.

[a] *College of Chemistry and Materials Engineering, Wenzhou University, Wenzhou, 325035, P. R. China. E-mail: xiaobhuang@wzu.edu.cn; huayuewu@wzu.edu.cn*
[b] *School of Chemistry and Chemical Engineering, Nanjing University, Nanjing, 210093, P. R. China. E-mail: yxcheng@nju.edu.cn*
Electronic Supplementary Information (ESI) available: UV-vis spectra, PL spectra, spectral data, fluorescence images, ^{1}H-NMR and ^{13}C-NMR. See
DOI: 10.1039/x0xx00000x

Recently, 4*H*-pyran has been widely used as a building block for constructing D-π-A-type fluorophores in red fluorescence materials, such as dicyanomethylene-4*H*-pyran (DCM) derivatives.[16] A series of DCM derivatives with twisted conformations have recently been reported to show obvious AIE activity originating from the restriction of intramolecular rotation (RIR).[17] A butterfly-shaped molecule based on a pyran skeleton and cholesteryl chains has also been reported to exhibit red fluorescence in the amorphous phase.[18] In this work, we designed and synthesized a series of D-π-A indene-1,3-dionemethylene-4*H*-pyran (IDMP) derivatives using indene-1,3-dionemethylene (IDM) as the electron acceptor and a phenyl ring containing different lengths of alkoxy chains as the electron donor. Herein, the introduction of the long alkoxy side chain onto the phenyl ring not only improves the dissolution properties of these compounds, but also might have significant effects on their aggregation behaviors in the solid state by changing the molecular backbone conformation and the molecular packing mode.[7,12b,12d,12f,19] We examined in detail the photophysical properties of the target compounds and their structure–property relationships. These IDMP derivatives show obvious AIEE phenomena in a THF/water mixture and emit from yellow to red fluorescence in the solid state. Furthermore, some of the compounds exhibit not only outstanding reversible MFC properties, but also alkoxy-chain-length-dependent aggregate fluorescence properties. Interestingly, a fluorescence colour change similar to that caused by MFC activity can also be achieved by a simple dissolution–desolvation process (DDP) in different solvent systems, such as chloroform and THF, which can be considered as a solvent-induced emission change. X-ray diffraction (XRD) experiments reveal that the MFC properties and solvent-induced emission changes by a DDP can be attributed to the transformation between crystalline and amorphous states under a particular stimulus, such as pressure or solvent.

Experimental

Measurements and materials

^{1}H and ^{13}C NMR spectra were recorded in solution of $CDCl_3$ on a Bruker DRX 500 NMR spectrometer with tetramethylsilane (TMS) as the internal standard. Electrospray ionization-mass spectrometry (ESI-MS) spectra were recorded on a Finnigan DECAX-30000 LCQ Deca mass spectrometer. MALDI-TOF MS spectra were recorded on a Bruker autoflex speed MALDI-TOF/TOF mass spectrometer. Fourier transform infrared (FT-IR) spectra were taken on a Nexus 870 FT-IR spectrometer. C, H and N of elemental analyses were performed on an Elementar Vario MICRO analyzer. UV-vis absorption spectra were recorded on a Perkine-Elmer Lambda 25 spectrometer. Fluorescence spectra were recorded on a HITACHI F-7000 fluorometer. Time-resolved emission decay behaviors were measured on a FluoroMax-4 (Horiba Jobin Yvon) fluorometer. Fluorescent microscopic images were taken with a Lecia DMI3000B inverted optical microscope. X-ray diffraction (XRD) measurements were performed by using a Bruker X-ray diffractometer (D8 Advance). 4-Methoxybenzaldehyde was obtained from Aldrich Chemical Co. and the other 4-alkoxybenzaldehyde were synthesized according to the previous literature.[20]

Synthesis of 2-(2,6-dimethyl-4*H*-pyran-4-ylidene)-1*H*-indene-1,3(2*H*)-dione (2)

2,6-Dimethyl-4-pyrone (**1**) (8.0 mmol, 0.99 g) and 2*H*-indene-1,3-dione (24.0 mmol, 3.5 g) in 15 mL of acetic anhydride were heated under reflux for 4 h. After cooling, K_2CO_3 was added to the reaction solution in batches, adjusting the pH value to neutral. The mixture was then extracted with ethyl acetate (2 × 100 mL). The combined organic layers were washed with water and brine, and then dried over anhydrous Na_2SO_4. After removal of solvent under reduced pressure, the crude product was purified by column chromatography (petroleum ether/ethyl acetate) (10:1, v/v) to afford pure compound **2** as a yellow solid (1.54 g, 75 %). ^{1}H NMR ($CDCl_3$, 500 MHz): δ 8.27 (s, 2H), 7.74 (dd, ^3J = 5.0 Hz, ^4J = 3.0 Hz, 2H), 7.58 (dd, ^3J = 5.5 Hz, ^4J = 3.0 Hz, 2H), 2.36 (s, 6H). ^{13}C NMR ($CDCl_3$, 125 MHz): δ 192.8, 164.8, 149.3, 140.6, 133.1, 121.3, 107.5, 107.3, 20.3.

General procedure for IDMP derivatives

A mixture of compound **2** (252.1 mg, 1.0 mmol), 4-alkoxybenzaldehyde (6.0 mmol), piperidine (0.5 mL), and CH_3CN (8 mL) were refluxed under argon for 24 h. After cooling to room temperature, the reaction mixture was poured into methanol (60 mL) and suction filtered to give the crude product. The crude product was washed with acetone and petroleum ether five times, respectively, and then dried to give the pure IDMP derivatives.

2-(2,6-Bis((*E*)-4-methoxystyryl)-4*H*-pyran-4-ylidene)-1*H*-indene-1,3(2*H*)-dione (3a). Orange-red solids (341.7 mg), 70% yield. ^{1}H NMR ($CDCl_3$, 500 MHz): δ 8.40 (s, 2H), 7.74 (dd, ^3J = 5.0 Hz, ^4J = 3.0 Hz, 2H), 7.58 (dd, ^3J = 5.0 Hz, ^4J = 3.0 Hz, 2H), 7.52 (d, J = 8.5 Hz, 4H), 7.45 (d, J = 16.0 Hz, 2H), 6.94 (d, J = 8.0 Hz, 4H), 6.75 (d, J = 16.0 Hz, 2H), 3.86 (s, 6H). ^{13}C NMR ($CDCl_3$, 125 MHz): δ 192.6, 161.1, 160.3, 148.3, 140.7, 136.0, 130.0, 129.3, 127.8, 121.2, 117.7, 114.5, 108.6, 108.3, 55.4. MS (ESI, m/z): 489.10 (M^++H). FT-IR (KBr, cm^{-1}): 3032, 2965, 1712, 1695, 1651, 1638, 1599, 1525, 1507, 1408, 1334, 1256, 1235, 1173, 953. Anal. calcd for $C_{32}H_{24}O_5$: C, 78.67; H, 4.95. Found: C, 78.61; H, 4.99.

2-(2,6-Bis((*E*)-4-ethoxystyryl)-4*H*-pyran-4-ylidene)-1*H*-indene-1,3(2*H*)-dione (3b). Orange-red solids (387.1 mg), 75% yield. ^{1}H NMR ($CDCl_3$, 500 MHz): δ 8.42 (s, 2H), 7.76 (dd, ^3J = 5.0 Hz, ^4J = 3.0 Hz, 2H), 7.60 (dd, ^3J = 5.0 Hz, ^4J = 3.0 Hz, 2H), 7.53 (d, J = 8.5 Hz, 4H), 7.47 (d, J = 16.0 Hz, 2H), 6.94 (d, J = 8.5 Hz, 4H), 6.77 (d, J = 16.0 Hz, 2H), 4.09 (q, J = 7.0 Hz, 4H), 1.45 (t, J = 7.0 Hz, 6H). ^{13}C NMR ($CDCl_3$, 125 MHz): δ 192.7, 160.6, 160.4, 148.4, 140.8, 136.1, 133.0, 129.3, 127.7, 121.2, 117.7, 115.0, 108.6, 108.3, 63.7, 14.8. MS (ESI, m/z): 517.15 (M^++H). FT-IR (KBr, cm^{-1}): 3040, 2924, 1713, 1687, 1649, 1636, 1599, 1526, 1502, 1404, 1332, 1251, 1231, 1173, 950. Anal. calcd for $C_{34}H_{28}O_5$: C, 79.05; H, 5.46. Found: C, 79.09; H, 5.41.

2-(2,6-Bis((*E*)-4-propoxystyryl)-4*H*-pyran-4-ylidene)-1*H*-indene-1,3(2*H*)-dione (3c). Orange-red solids (435.4 mg), 80% yield. ^{1}H NMR ($CDCl_3$, 500 MHz): δ 8.37 (s, 2H), 7.71 (dd, ^3J = 5.0 Hz, ^4J = 3.0 Hz, 2H), 7.56 (dd, ^3J = 5.0 Hz, ^4J = 3.0 Hz, 2H), 7.49 (d, J = 9.0 Hz, 4H), 7.41 (d, J = 16.0 Hz, 2H), 6.90 (d, J = 8.5 Hz, 4H), 6.71 (d, J = 16.0 Hz, 2H), 3.95 (t, J = 6.5 Hz, 4H), 1.87-1.80 (m, 4H), 1.06 (t, J = 7.5 Hz, 6H). ^{13}C NMR ($CDCl_3$, 125 MHz): δ 192.6, 160.8, 160.5, 148.4, 140.8,

136.1, 133.0, 129.3, 127.7, 121.2, 117.6, 115.0, 108.6, 108.3, 69.7, 22.5, 10.5. MS (ESI, m/z): 545.20 (M^++H). FT-IR (KBr, cm^{-1}): 2963, 1712, 1694, 1653, 1637, 1598, 1530, 1507, 1406, 1331, 1254, 1233, 1169, 951. Anal. calcd for $C_{36}H_{32}O_5$: C, 79.39; H, 5.92. Found: C, 79.32; H, 5.99.

2-(2,6-Bis((*E*)-4-butoxystyryl)-4*H*-pyran-4-ylidene)-1*H*-indene-1,3(2*H*)-dione (3d). Orange-red solids (412.0 mg), 72% yield. ^{1}H NMR ($CDCl_3$, 500 MHz): δ 8.32 (s, 2H), 7.68 (dd, ^3J = 5.0 Hz, ^4J = 3.0 Hz, 2H), 7.53 (dd, ^3J = 5.0 Hz, ^4J = 3.0 Hz, 2H), 7.44 (d, J = 8.5 Hz, 4H), 7.35 (d, J = 16.0 Hz, 2H), 6.86 (d, J = 8.5 Hz, 4H), 6.66 (d, J = 16.0 Hz, 2H), 3.96 (t, J = 6.0 Hz, 4H), 1.81-1.76 (m, 4H), 1.54-1.47 (m, 4H), 1.00 (t, J = 7.5 Hz, 6H). ^{13}C NMR ($CDCl_3$, 125 MHz): δ 192.5, 160.7, 160.4, 148.3, 140.7, 136.0, 132.9, 129.3, 127.6, 121.2, 117.5, 114.9, 108.5, 108.3, 67.8, 31.2, 19.2, 13.8. MS (ESI, m/z): 573.25 (M^++H). FT-IR (KBr, cm^{-1}): 3036, 2956, 1713, 1693, 1651, 1636, 1597, 1532, 1506, 1404, 1331, 1252, 1232, 1174, 949. Anal. calcd for $C_{38}H_{36}O_5$: C, 79.70; H, 6.34. Found: 79.75; H, 6.29.

2-(2,6-Bis((*E*)-4-(octyloxy)styryl)-4*H*-pyran-4-ylidene)-1*H*-indene-1,3(2*H*)-dione (3e). Orange solids (485.9 mg), 71% yield. ^{1}H NMR ($CDCl_3$, 500 MHz): δ 8.43 (s, 2H), 7.76 (dd, ^3J = 5.0 Hz, ^4J = 3.0 Hz, 2H), 7.60 (dd, ^3J = 5.0 Hz, ^4J = 3.0 Hz, 2H), 7.54 (d, J = 8.0 Hz, 4H), 7.48 (d, J = 16.0 Hz, 2H), 6.94 (d, J = 8.5 Hz, 4H), 6.78 (d, J = 16.0 Hz, 2H), 4.01 (t, J = 6.0 Hz, 4H), 1.84-1.78 (m, 4H), 1.50-1.45 (m, 4H), 1.38-1.26 (m, 16H), 0.90 (t, J = 7.0 Hz, 6H). ^{13}C NMR ($CDCl_3$, 125 MHz): δ 192.5, 160.7, 160.4, 148.3, 140.7, 136.0, 132.9, 129.3, 127.6, 121.4, 117.5, 114.9, 108.5, 108.3, 68.2, 31.8, 29.3, 29.2, 29.1, 26.0, 22.6, 14.1. MS (ESI, m/z): 685.32 (M^++H). FT-IR (KBr, cm^{-1}): 3039, 2922, 1713, 1691, 1651, 1636, 1597, 1506, 1404, 1332, 1249, 1233, 1170, 949. Anal. calcd for $C_{46}H_{52}O_5$: C, 80.67; H, 7.65. Found: C, 80.60; H, 7.62.

2-(2,6-Bis((*E*)-4-(dodecyloxy)styryl)-4*H*-pyran-4-ylidene)-1*H*-indene-1,3(2*H*)-dione (3f). Orange solids (605.3 mg), 76% yield. ^{1}H NMR ($CDCl_3$, 500 MHz): δ 8.34 (s, 2H), 7.69 (dd, ^3J = 5.5 Hz, ^4J = 3.5 Hz, 2H), 7.53 (dd, ^3J = 5.5 Hz, ^4J = 3.5 Hz, 2H), 7.46 (d, J = 8.0 Hz, 4H), 7.38 (d, J = 16.0 Hz, 2H), 6.87 (d, J = 8.0 Hz, 4H), 6.68 (d, J = 16.0 Hz, 2H), 3.96 (t, J = 6.5 Hz, 4H), 1.82-1.76 (m, 4H), 1.48-1.43 (m, 4H), 1.36-1.27 (m, 32H), 0.89 (t, J = 7.0 Hz, 6H). ^{13}C NMR ($CDCl_3$, 125 MHz): δ 192.5, 160.8, 160.4, 148.3, 140.7, 136.0, 132.9, 129.3, 127.6, 121.2, 117.6, 114.9, 108.6, 108.3, 68.2, 31.9, 29.7, 29.6, 29.59, 29.57, 29.4, 29.3, 29.2, 26.0, 22.7, 14.1. MS (ESI, m/z): 797.35 (M^++H). FT-IR (KBr, cm^{-1}): 3070, 2919, 2851, 1712, 1691, 1651, 1639, 1598, 1533, 1503, 1406, 1330, 1254, 1232, 1172, 953. Anal. calcd for $C_{54}H_{68}O_5$: C, 81.37; H, 8.60. Found: C, 81.32; H, 8.65.

2-(2,6-Bis((*E*)-4-(hexadecyloxy)styryl)-4*H*-pyran-4-ylidene)-1*H*-indene-1,3(2*H*)-dione (3g). Orange solids (708.7 mg), 78% yield. ^{1}H NMR ($CDCl_3$, 500 MHz): δ 8.43 (s, 2H), 7.77 (dd, ^3J = 5.0 Hz, ^4J = 3.0 Hz, 2H), 7.60 (dd, ^3J = 5.0 Hz, ^4J = 3.0 Hz, 2H), 7.54 (d, J = 8.5 Hz, 4H), 7.48 (d, J = 16.0 Hz, 2H), 6.95 (d, J = 8.5 Hz, 4H), 6.78 (d, J = 16.0 Hz, 2H), 4.01 (t, J = 6.5 Hz, 4H), 1.84-1.78 (m, 4H), 1.50-1.44 (m, 4H), 1.38-1.26 (m, 48H), 0.88 (t, J = 7.0 Hz, 6H). ^{13}C NMR ($CDCl_3$, 125 MHz): δ 192.5, 160.8, 160.4, 148.3, 140.7, 136.0, 132.9, 129.3, 127.6, 121.2, 117.6, 114.9, 108.6, 108.3, 68.2, 31.9, 29.69, 29.66, 29.65, 29.60, 29.58, 29.4, 29.3, 29.2, 26.0, 22.7, 14.1. FT-IR (KBr, cm^{-1}): 3071, 2918, 2850, 1691, 1651, 1639, 1598, 1534, 1505, 1406, 1329, 1254, 1232, 1172, 953. MALDI-TOF MS: $C_{62}H_{84}O_5$, calcd 908.6319; Found 908.2431.

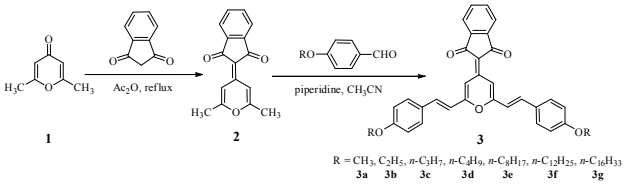

Scheme 1 Synthetic route for IDMP derivatives **3**.

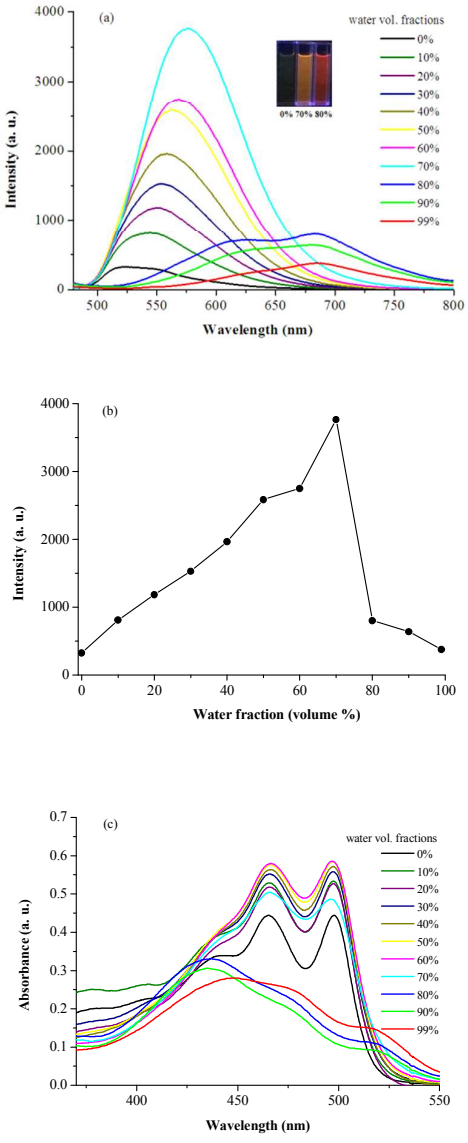

Fig. 1 (a) Fluorescence spectra of **3a** (1×10^{-5} mol/L) in THF/water mixtures with different f_w values. Insets: Visible fluorescence of **3a** (1×10^{-5} mol/L) in 0%, 70%, and 80% water under a 365-nm UV lamp. (b) The plot of fluorescence peak intensity of **3a** in THF/water mixtures against f_w values. (c) UV-vis spectra of **3a** (1×10^{-5} mol/L) in THF/water mixtures with different f_w values.

Results and discussion

Synthesis and features of IDMP derivatives

Scheme 1 illustrates the synthetic route to IDMP derivatives **3**. 2-(2,6-Dimethyl-4*H*-pyran-4-ylidene)-2*H*-indene-1,3-dione (**2**) was synthesized by the reaction of 2,6-dimethyl-4-pyrone (**1**) with 2*H*-indene-1,3-dione in acetic anhydride.[21] The IDMP derivatives **3** were synthesized using the Knoevenagel condensation reaction of compound **2** with 4-alkoxybenzaldehyde in CH_3CN at 80°C in 70–80% yield. According to the ^{1}H NMR spectra data of these target compounds, the chemical shifts of the H atoms in the ethylene units show two groups of peaks at about 7.40 ppm and 6.70 ppm with ^3J values of 16.0 Hz, which indicates that these compounds should exist in the *E* isomeric form. The resulting compounds are soluble in common organic solvents such as $CHCl_3$, THF, and CH_2Cl_2, but insoluble in methanol and water.

AIEE properties of IDMP derivatives

The UV-vis absorption and emission spectra of the IDMP derivatives were measured in THF as shown in Fig. S1 and the data are presented in Table S1. The results show these compounds have similar absorption and emission spectra, and exhibit three absorption peaks in the range of 441–500 nm, and two emission peaks in the range of 523–447 nm. Considering that the only difference between these molecules is the length of the alkoxy chain, it can be concluded that the length has no obvious influence on the absorption and emission spectra in the THF solution.

To determine whether these IDMP derivatives have AIEE properties, their absorption and emission behaviors in solvent–nonsolvent mixtures were studied. These compounds are insoluble in water while soluble in THF. Adding water to the THF solutions of these compounds will cause the well-dissolved molecules to aggregate and result in changes to their absorption and emission spectra. As shown in Fig. 1a, when compound **3a** was dissolved in THF, its dilute pure THF solution (1×10^{-5} mol/L) emitted weak yellow-green light at 524 nm and 544 nm, which could be ascribed to the free rotation of the phenyl ring and IDMP ring linked to the axes of the olefinic double bonds *via* rotatable carbon–carbon single bonds and the resultant nonradiative relaxation process.[5,22] With increasing water volume fraction (f_w) values from 10 to 70%, the fluorescence intensity of the solution of **3a** increased gradually and reached the maximum emission intensity at 70% water fraction, which was about 12 times higher than that in pure THF. At the same time, the corresponding emission peak showed a 52-nm redshift from 523 nm to 575 nm. The increase in fluorescence intensity and the redshift of the emission wavelength could be attributed to the RIR and to some extent, the probable conformation planarization in the aggregates.[12c,23] This result indicated that **3a** exhibited obvious AIEE activity. Similar AIEE phenomena were observed for the other IDMP derivatives (Fig. S2). With the increasing water content, the fluorescence intensities of the other IDMP derivatives in the THF/water mixtures reached maximum values at 70% (for **3b**), 60% (for **3c** and **3d**), and 50% (for **3e**–**3g**), respectively. The fluorescence intensities showed either a gradual decrease or a complicated zigzag-type change with the further increase of the water fraction, as shown in Fig. 1 and Fig. S2. The complex changes in the emission peak intensities versus water fractions for these compounds were often observed in other reports of AIEE compounds,[11a,12a,12g,19a] but the reasons remained unclear. Possible reasons for this phenomenon are explained as follows: At a "low" water fraction, the well-dispersed molecules in THF begin to aggregate and restrain the intramolecular rotations, resulting in gradual enhancement of the fluorescence. By further increasing the water fraction, the solute molecules might aggregate into crystal particles and amorphous particles.[24] The measured fluorescence intensity depends on the combined actions of the two types of nanoparticles, crystalline particles lead to an enhancement in the emission intensity, while amorphous particles cause a reduction in intensity.[11a] Because the formation of nanoparticles is hard to control in "high" water content, the measured fluorescence intensity often shows a complex change.

The absorption spectra of **3a** in the THF/water mixtures (1×10^{-5} mol/L) are shown in Figure 1c. It was found that the spectral profiles showed an obvious decrease when $f_w \geq 70\%$. Meanwhile, there were level-off tails in the visible region, which could be attributed to light-scattering effects and indicated the formation of aggregates.[25] Similar results were observed in **3b**–**3g** (Fig. S3). It was also found that the absorption spectra of the compounds in the THF/water mixture with higher f_w values exhibited some differences in absorption band shapes and maxima, which might be attributed to the formation of different aggregated states of the molecules.

To gain insight into the possible RIR mechanism of AIEE, we first investigated the emission behavior of **3a** in methanol/glycerol mixtures (1×10^{-5} mol/L, containing 0.5 vol% THF) with different fractions of glycerol. According to a previous report,[26] if a RIR process was at work, the AIE/AIEE molecules should become more luminescent in their solutions with increasing solution viscosity because the thickening was known to hamper intramolecular rotations. It was found that the emission of **3a** in the methanol/glycerol mixture gradually enhanced with increasing

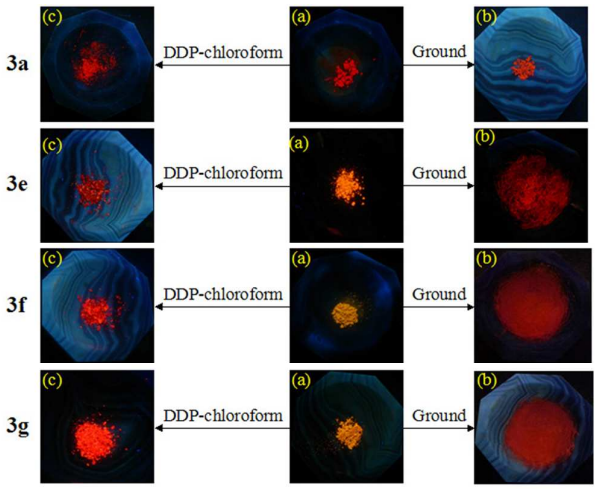

Fig. 2 Fluorescence images of **3a** and **3e**–**3g** solid samples taken under a 365-nm UV lamp: (a) as-synthesized samples; (b) ground samples; (c) DDP-chloroform samples.

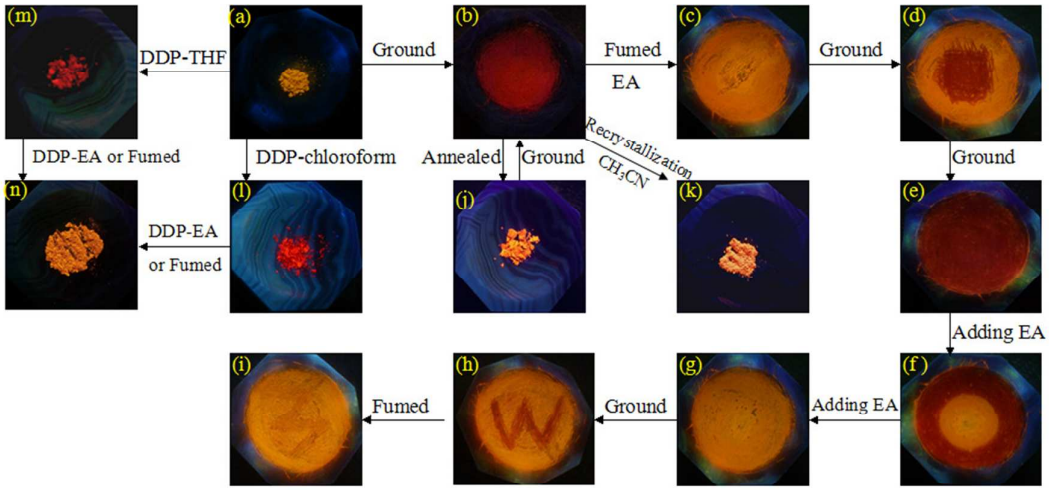

Fig. 3 Fluorescence images of solid samples of **3f** taken under a 365-nm UV lamp: (a) as-synthesized samples; (b) ground samples; (c) fumed samples; (d) the central part of fumed samples was ground; (e) all fumed samples were ground; (f) several drops of EA were dropped onto the ground samples; (g) all ground samples were soaked with EA; (h) and (i) **3f** is used to write "W" with a metal spatula and then fumed using EA; (j) annealed samples; (k) recrystallized samples using CH_3CN as a solvent; (l) DDP-chloroform samples; (m) DDP-THF samples; (n) DDP-EA samples or fumed samples using EA.

amounts of glycerol, and the emission intensity at 90% glycerol fraction was about 20 times higher than that in methanol solution (Fig. S4). Additionally, the emission wavelengths showed little change with increasing glycerol fraction, which indicated that the emission enhancement was predominantly due to the viscosity effect and not the aggregation of the molecules. These results indicated that increasing the viscosity of the solvent mixture could effectively enhance the emission of **3a**, suggesting that the AIEE of **3a** was caused by the RIR process. We further investigated the emission behaviors of **3d** and **3f** in methanol/glycerol mixtures and found that the fluorescence intensities reached maximum values at 60% and 20% glycerol content, respectively (Fig. S4). It was intriguing that the amount of added glycerol for reaching the corresponding maximum emission intensities decreased in a sequence of **3a** > **3d** > **3f**, which implied that the longer the alkoxy chain, the less glycerol needed. The possible reason is that the longer alkoxy chain is advantageous to earlier aggregation of the molecules. In fact, a similar phenomenon was observed in the emission behaviors of the IDMP derivatives in THF/water mixtures (Fig. 1 and Fig. S2). Subsequently, with further increase of the glycerol fraction, the fluorescence spectra of **3d** and **3f** in the methanol/glycerol mixtures showed obvious decrease and redshift, which could be attributed to the formation of a large number of amorphous aggregates and decreased solubility.

Considering the D-π-A structures of the IDMP derivatives, it is necessary to discuss the possible influence of the ICT process on their AIEE behaviors. It is well known that the ICT effect is associated with a remarkable bathochromic shift and decreased fluorescence with increasing solvent polarities. We measured the fluorescence spectra of **3a** in a series of solvents with increasing polarities, such as $CHCl_3$, THF, CH_2Cl_2, DMSO, and DMF (Fig. S5). It was found that the emission wavelength of **3a** had a certain degree of redshift as the polarity of the solvents increased, however, the emission intensity showed obvious enhancement when DMSO and DMF were used as solvents, which indicated that **3a** did not show a typical ICT effect in these solutions. Additionally, we investigated the fluorescence behavior of **3a** in THF/DMF mixtures with different DMF fractions. The solvent polarity of DMF is higher than that of THF, thus, increasing the DMF fractions in the mixed solvents would increase the polarity of the mixture. However, as shown in Fig. S5, the fluorescence spectra in this mixture system exhibited obvious fluorescence enhancement with the increase of DMF fraction and the ICT effect was not obvious. The results indicate that the fluorescence enhancement of **3a** in the THF/water system could be attributed to a RIR mechanism accompanied by a limited ICT effect.[5,13b,14]

MFC properties and solvent-induced emission changes of IDMP derivatives

As shown in Fig. 2 and Fig. S6, the as-synthesized solids **3a–3g** emitted strong red, orange–red, orange, and yellow fluorescence under a 365-nm UV lamp, and the emissions were gradually blueshifted from red to yellow with the increase of the alkoxy chain length. The fluorescence quantum yields (Φ_F) of the IDMP solids were in the range of 2.5-7.1% (Table S2). When these as-synthesized solid samples were ground with a pestle in a mortar, it was found that fluorescence colour changes were not obvious for **3a–3d**, however, the changes could be clearly observed from orange (**3e**) or yellow (**3f**, **3g**) to red, which indicated that the longer the alkoxy chains, the bigger the fluorescence colour difference induced by grinding. As a result, **3e–3g** containing the longer chains showed more evident MFC properties compared with that of **3a–3d** containing shorter chains. In addition, the colours of the ground samples under natural light also exhibited an alkoxy-length-dependent phenomenon, which indicated that the pressure changes not only the emission spectra but also the absorption spectra (Fig. S7). Using **3f** containing a dodecyloxy chain as an example, we further investigated the changes of the colours in the solid state upon various external stimuli (Fig. 3, Fig. S8). When the ground samples of **3f** were annealed at a temperature (80 °C) below the isotropic melting point for 30 min, when ethyl acetate (EA) was directly added in the mortar, or the sample was exposed to EA vapour at room temperature, the fluorescence colours were all almost converted to the colours of the as-synthesized samples, thus demonstrating good reversibility in the emission spectra.

Table 1 Peak emission wavelengths (nm) of solid-state IDMP derivatives under different conditions.

Compound	$\lambda_{As\text{-}synthesized}$	λ_{Ground}	$\lambda_{DDP\text{-}chloroform}$	$\Delta\lambda_{MFC}$ [a]	$\Delta\lambda_{DDP\text{-}chloroform}$ [b]	$\lambda_{DDP\text{-}THF}$	$\lambda_{DDP\text{-}EA}$	$\lambda_{Recrystallized}$	$\lambda_{Annealed}$
3a	640	645	649	5	9	n.d. [c]	n.d.	n.d.	n.d.
3b	627	628	638	1	11	n.d.	n.d.	n.d.	n.d.
3c	609	610	613	1	4	n.d.	n.d.	n.d.	n.d.
3d	602	609	612	7	10	n.d.	n.d.	n.d.	n.d.
3e	589	637	647	48	57	n.d.	n.d.	n.d.	n.d.
3f	567	611	633	44	66	644	580	572	575
3g	580	631	621	51	41	n.d.	n.d.	n.d.	n.d.

[a] $\Delta\lambda_{MFC} = \lambda_{Ground}-\lambda_{As\text{-}synthesized}$. [b] $\Delta\lambda_{DDP\text{-}chloroform} = \lambda_{DDP\text{-}chloroform}-\lambda_{As\text{-}synthesized}$. [c] n.d. = no detection.

Furthermore, the fluorescence colour of ground samples of **3f** could also be recovered by a recrystallization process using CH_3CN as a solvent. Interestingly, if the as-synthesized samples of **3e**–**3g** were dissolved in chloroform or THF and then evaporated to dryness *via* vacuum rotary evaporation, strong red-emitting solids were obtained, which was similar to those showing MFC properties and could be ascribed to solvent-induced emission changes caused by a simple DDP. The solid samples obtained by the DDP using chloroform or THF could be nearly converted to the original samples by fuming or another DDP using EA as the solvent. The results indicated that **3f** in the solid state had reversible colour change features. When the letter "W" was written on the surface of the as-synthesized solids using a metal spatula, the colour change occurred only on the written area, indicating that **3f** was a high-contrast MFC material. Similar reversible colour changes under natural and UV light could be observed in **3e** and **3g** under particular stimuli (Fig. S9 and Fig. S10).

The emission spectra of the as-synthesized samples of the IDMP solids were measured and their maximum emission wavelengths were found to be in the range of 640–567 nm, showing an obvious blueshift with the increase of the alkoxy chain length (Table 1, Fig. S11). The gradual blueshift of the emission spectra might be attributed to the fact that the compounds with the long chains have a more distorted conformation and weaker conjugation than those compounds containing short chains.[19a] The results indicated that the alkoxy chain could significantly influence the solid-state aggregation behaviors of IDMP derivatives, which was quite different from the results in solution. The emission spectra of as-synthesized samples of these compounds under various external stimuli are depicted in Fig. 4 (**3f**) and Fig. S12 (**3a**–**3e**, **3g**), and the corresponding data are summarized in Table 1. With regard to **3a**–**3d**, it was found that the maximum emission wavelengths of the ground samples and the DDP-chloroform samples exhibited a small redshift compared with the corresponding as-synthesized samples ($\Delta\lambda$ = 1–11 nm). Considering that the as-synthesized samples emitted red or orange–red fluorescence, the colour changes were not as obvious to the naked eye, and therefore **3a**–**3d** could not exhibit obvious MFC properties. Unlike **3a**–**3d**, a significant redshift ($\Delta\lambda$ = 41–66 nm) could be observed in **3e**–**3g**, and an obvious fluorescence colour change from orange (**3e**) and yellow (**3f**, **3g**) to red was very obvious. These results implied that the IDMP derivatives were chain-length-dependent MFC materials, and the alkoxy chain played a functional role in tuning their MFC behaviors. It was noted that the longer the alkoxy chain, the more remarkable the MFC behavior, indicating that a longer alkoxy chain was beneficial for effective mechanofluorochromism of these IDMP derivatives. The UV-vis absorption spectra also showed that the longer alkoxy chains had greater impact on the aggregation state of the solid samples of the IDMP derivatives (Fig. S13). For **3f**, the emission spectra of the ground samples showed a 44-nm redshift compared with those of the as-synthesized samples. When **3f** was treated by a DDP using different solvents, the maximum emission wavelengths of the DDP-chloroform samples and the DDP-THF samples showed a 66- and 77-nm redshift, respectively. However, those of DDP-EA samples only showed a 13-nm redshift, and therefore EA could be used as fuming vapor to recover the fluorescence of the solids. The results indicated that aggregates with different morphology were formed in the DDP using different solvent systems. After the ground samples of **3f** were annealed or recrystallized using CH_3CN as a solvent, the fluorescence wavelengths were blueshifted by 36 nm and 39 nm, respectively, and were fully unable to return to the wavelengths of the as-synthesized samples. However, the reversible colour changes were clearly observed in annealed-ground or fumed-ground samples. The results indicate that **3f** is a promising candidate for temperature-, vapour-, or pressure-sensing systems and optical recording.

To gain an insight into the mechanism of the MFC effect and solvent-induced emission properties caused by the DDP, XRD measurements of the various IDMP solid samples were performed (Fig. 5 and Fig. S14). As shown in Fig. 5, the diffraction curve of the as-synthesized sample of **3f** revealed many sharp and intense reflections, indicative of a well-ordered microcrystalline structure. After the as-synthesized sample was treated by external stimuli, most diffraction peaks remarkably weakened or disappeared, indicating significant damage of the self-assembled architecture to an amorphous state. In agreement with this, the treated sample showed bigger emission wavelength and lower Φ_F than that in the as-synthesized state (Table S2). The morphology changes of the **3e** and **3f** solids from a crystalline state to an amorphous state could also be seen in the fluorescence microscope images (Fig. S15). The XRD curve diffraction peaks, and hence the crystalline structure, could be recovered after fuming, annealing, or recrystallization, which resulted in the blue shifts in the fluorescence spectra. The results showed that the significant MFC properties and solvent-

induced emission changes can be attributed to the structural changes in molecular aggregation from the crystalline state to the amorphous state, and could be thought of as altered-morphology-induced emission properties. Similar phenomena were observed for other IDMP solid samples (Fig. S14). It could be found that there were part crystalline features in the XRD curves of some ground samples, which could be caused by incomplete phase transition. It was noted that the solids of **3a–3d** also had the transformation of crystalline and amorphous state under the external stimuli; however, the change from red to more red could hardly be distinguished with the naked eye. Herein, a possible mechanism for the altered-morphology-induced emission phenomenon of these IDMP derivatives is proposed. The twisted conformation of molecules can result in relatively loose molecular packing and numerous defects of their aggregates, which easily destroys crystalline aggregates by planarization of the molecular conformation or slip deformation under external pressure, thereby increasing molecular conjugation and facilitating a redshift of the fluorescence spectra.[1a,12g] With regard to the alkoxy length dependence of altered-morphology-induced emission, one probable explanation is that the compounds containing longer chains have more distorted conformations and weaker supramolecular interactions and as a result more relaxed molecular stacking and lower lattice energies compared with those containing a short alkoxy chain.[19a]

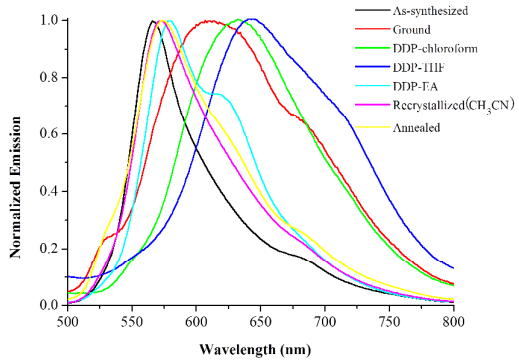

Fig. 4 Fluorescence spectra of **3f** solid samples under different conditions.

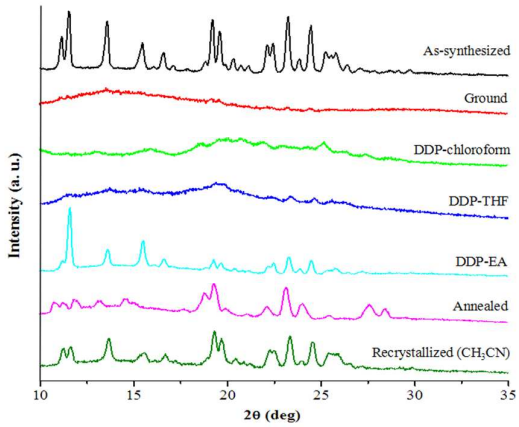

Fig. 5 XRD curves of **3f** solid samples under different conditions.

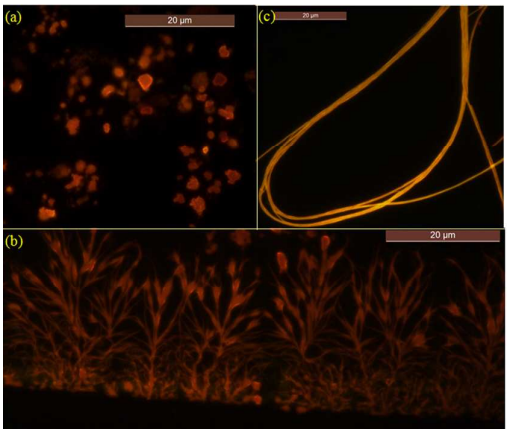

Fig. 6 The fluorescence microscope images of **3f** in a THF/water mixture (1×10^{-5} mol/L) at different f_w values: (a) f_w = 20%; (b) f_w = 30%; (c) f_w = 50%.

The time-resolved emission decay behaviors of these IDMP derivatives under different conditions, such as by grinding and a DDP, were studied (Table S2). It was found that there were all two relaxation pathways for the fluorescence decay of these compounds, which indicated that the time-resolved fluorescence spectra of these compounds included independent emissions because multiple lifetimes were detected. With regard to **3e–3g**, the weighted mean lifetime <τ> values under different conditions were significantly different. It could be concluded that if the materials had significant altered-morphology-induced emission, the time-resolved emission decay behaviors of the samples under different conditions exhibited distinct changes, which were consistent with the results reported by the previous literatures.[11a,12g] It was noted that the <τ> values of **3a** and **3b** also showed a certain degree of changes, indicating that there were the transformation of crystalline and amorphous state under the external stimuli, which was consistent with the results of the XRD measurements.

Self-assembly

As discussed above, the experimentally observed AIEE phenomenon and MFC properties indicate that IDMP derivatives adopt twisted conformations that prevent intermolecular π–π stacking and exhibit different morphology upon external stimuli. Without large planar cores in these molecules, a dipole–dipole interaction can also be used to achieve ordered self-assemblies.[27] Herein, we explored the morphologies of the microparticles of **3f** formed in THF/water mixtures (1×10^{-5} mol/L) with various f_w values (Fig. 6). As displayed in Fig. 6, numerous block crystalline microparticles emitting orange red light were observed at f_w = 20% and the diameters were several micrometers. When f_w was increased to 30%, some dendritic microribbons began to form, some block microparticles were dotted at the top and bottom of the branches, and the shape was just like flowering monochoria vaginalis. At f_w = 50%, long and thin

microribbons were formed and emitted orange–yellow fluorescence. However, no ordered microstructures could be observed at higher water volume fractions. At a "low" water fraction, the molecular aggregation process was slow and resulted in large microcrystallines. The aggregation process was sped up with the increase of water volumes and the sizes of the aggregates became smaller and thinner. Additionally, it was found that the aggregates of **3d** and **3e** at f_w = 70% both showed ordered microcrystallines (Fig. S16). In sharp contrast, block crystalline microparticles and amorphous filamentous aggregates were simultaneously generated in the THF/water mixtures of **3g** when f_w was 30%, and then block microparticles were interspersed in the middle of the threads because of the fast precipitation rate when f_w was increased to 70%, appearing as irregular filaments algae. The results indicate that the longer alkoxy chain is advantageous to faster aggregation of the molecules and leads to the formation of irregular microparticles, which is consistent with the fluorescence behaviors of these compounds in the THF/water mixtures. Therefore, the coexistence of crystal and amorphous aggregates can serve as a reason for the complexity of the AIEE phenomenon of these compounds in the THF/water mixtures.

Conclusions

In this work, we synthesized a series of D-π-A IDMP derivatives using indene-1,3-dionemethylene as an electron acceptor and a phenyl ring containing different lengths of alkoxy chains as an electron donor to investigate their photophysical properties. The results show that IDMP derivatives exhibit an obvious AIEE effect because of the restriction of intramolecular rotation in the aggregate state. It can be found that the length of the alkoxy chain has obvious influence on the emission behaviors of these compounds in THF/water or glycerol/methanol mixtures, that is, the longer alkoxy chain is advantageous to faster aggregation of the molecules and causes the fluorescence intensity to reach the maximum value at smaller f_w. This can also be confirmed by their self-assembly behaviors in THF/water mixtures. The as-synthesized IDMP solids emitted from red to yellow fluorescence and the fluorescence emissions showed obvious blueshifts with the increase of the length of the alkoxy chains. Some of these compounds exhibited obvious redshift MFC properties that were clearly alkoxy-length dependent: the longer the alkoxy chain, the more remarkable the MFC properties. Furthermore, the fluorescence emissions of these compounds could be altered by various external stimuli such as grinding, annealing, and solvent fuming. Interestingly, the solvent-induced emission redshift could be achieved by a simple DDP using chloroform or THF as the solvent. X-ray diffraction experiments revealed that the MFC properties and solvent-induced emission changes could both be considered as altered-morphology-induced emission properties that were ascribed to the crystalline-amorphous phase transformation under various external stimuli. The results indicate that the subtle manipulation of the length of the alkoxy chain of IDMP derivatives can endow them with unique and tunable solid-state optical properties.

Acknowledgements

This work was supported by the National Natural Science Foundation of China (Nos. 21204066, 21474048, and 21572165).

Notes and references

1 (a) Z. Chi, X. Zhang, B. Xu, X. Zhou, C. Ma, Y. Zhang, S. Liu and J. Xu, *Chem. Soc. Rev.*, 2012, **41**, 3878−3896; (b) S. Varughese, *J. Mater. Chem. C*, 2014, **2**, 3499–3516.

2 (a) S. J. Toal, K. A. Jones, D. Magde and W. C. Trogler, *J. Am. Chem. Soc.*, 2005, **127**, 11661−11665; (b) Z. Ning, Z. Chen, Q. Zhang, Y. Yan, S. Qian, Y. Cao and H. Tian, *Adv. Funct. Mater.*, 2007, **17**, 3799−3807; (c) B. Xu, M. Xie, J. He, B. Xu, Z. Chi, W. Tian, L. Jiang, F. Zhao, S. Liu, Y. Zhang, Z. Xu and J. Xu, *Chem. Commun.*, 2013, **49**, 273−275.

3 (a) S. Hirata and T. Watanabe, *Adv. Mater.*, 2006, **18**, 2725−2729; (b) S. J. Lim, B. K. An, S. D. Jung, M. A. Chung and S. Y. Park, *Angew. Chem. Int. Ed.*, 2004, **43**, 6346−6350; (c) K. Ariga, T. Mori and J. P. Hill, *Adv. Mater.*, 2012, **24**, 158−176.

4 (a) A. Kishimura, T. Yamashita, K. Yamaguchi and T. Aida, *Nat. Mater.*, 2005, **4**, 546−549; (b) H. Ito, T. Saito, N. Oshima, N. Kitamura, S. Ishizaka, Y. Hinatsu, M. Wakeshima, M. Kato, K. Tsuge and M. Sawamura, *J. Am. Chem. Soc.*, 2008, **130**, 10044−10045.

5 J. Luo, Z. Xie, J. W. Y. Lam, L. Cheng, H. Chen, C. Qiu, H. S. Kwok, X. Zhan, Y. Liu, D. Zhu and B. Z. Tang, *Chem. Commun.*, 2001, 1740−1741.

6 B. K. An, S. K. Kwon, S. D. Jung and S. Y. Park, *J. Am. Chem. Soc.*, 2002, **124**, 14410−14415.

7 L. Bu, M. Sun, D. Zhang, W. Liu, Y. Wang, M. Zheng, S. Xue and W. Yang, *J. Mater. Chem. C*, 2013, **1**, 2028–2035.

8 S. J. Yoon, J. W. Chung, J. Gierschner, K. S. Kim, M. G. Choi, D. Kim and S. Y. Park, *J. Am. Chem. Soc.*, 2010, **132**, 13675–13683.

9 (a) S. J. Yoon and S. Y. Park, *J. Mater. Chem.*, 2011, **21**, 8338–8346; (b) C. Dou, L. Han, S. Zhao, H. Zhang and Y. Wang, *J. Phys. Chem. Lett.*, 2011, **2**, 666–670; (c) X. Zhang, Z. Ma, M. Liu, X. Zhang, X. Jia and Y. Wei, *Tetrahedron*, 2013, **69**, 10552–10557; (d) J. Kunzelman, M. Kinami, B. R. Crenshaw, J. D. Protasiewicz and C. Weder, *Adv. Mater.*, 2008, **20**, 119–122; (e) Y. Zhang, G. Zhuang, M. Ouyang, B. Hu, Q. Song, J. Sun, C. Zhang, C. Gu, Y. Xu and Y. Ma, *Dyes Pigm.*, 2013, **98**, 486–492; (f) X. Zhang, Z. Ma, Y. Yang, X. Zhang, X. Jia and Y. Wei. *J. Mater. Chem. C*, 2014, **2**, 8932–8938.

10 X. Luo, J. Li, C. Li, L. Heng, Y. Q. Dong, Z. Liu, Z. Bo and B. Z. Tang, *Adv. Mater.*, 2011, **23**, 3261–3265.

11 (a) X. Zhang, Z. Chi, B. Xu, C. Chen, X. Zhou, Y. Zhang, S. Liu and J. Xu, *J. Mater. Chem.*, 2012, **22**, 18505–18513; (b) X. Zhou, H. Li, Z. Chi, X. Zhang, J. Zhang, B. Xu, Y. Zhang, S. Liu and J. Xu, *New J. Chem.*, 2012, **36**, 685–693; (c) X. Zhang, Z. Chi, H. Li, B. Xu, X. Li,W. Zhou, S. Liu, Y. Zhang and J. Xu, *Chem. Asian J.*, 2011, **6**, 808–811; (d) X. Luo, W. Zhao, J. Shi, C. Li, Z. Liu, Z. Bo, Y. Q. Dong and B. Z. Tang, *J. Phys. Chem. C*, 2012, **116**, 21967–21972; (e) N. Zhao, Z. Yang, J. W. Lam, H. H. Sung, N. Xie, S. Chen, H. Su, M. Gao, I. D. Williams, K. S. Wong and B. Z. Tang, *Chem. Commun.*, 2012, **48**, 8637–8639; (f) Q. Qi, J. Zhang, B. Xu, B. Li, S. X.-A. Zhang and W. Tian, *J. Phys. Chem. C*, 2013, **117**, 24997–25003; (g) Q. Qi, X. Fang, Y. Liu, P. Zhou, Y. Zhang, B. Yang, W. Tian and S. X.-A. Zhang, *RSC Adv.*, 2013, **3**, 16986–16989; (h) B. Xu, J. He, Y. Mu, Q. Zhu, S. Wu, Y. Wang, Y. Zhang, C.

Jin, C. Lo, Z. Chi, A. Lien, S. Liu and J. Xu, *Chem. Sci.*, 2015, **6**, 3236–3241.

12 (a) X. Zhang, Z. Chi, J. Zhang, H. Li, B. Xu, X. Li, S. Liu, Y. Zhang and J. Xu, *J. Phys. Chem. B*, 2011, **115**, 7606–7611; (b) Y. Wang, W. Liu, L. Bu, J. Li, M. Zheng, D. Zhang, M. Sun, Y. Tao, S. Xue and W. Yang, *J. Mater. Chem. C*, 2013, **1**, 856–862; (c) W. Liu, J. Wang, Y. Gao, Q. Sun, S. Xue, W. Yang, *J. Mater. Chem. C*, 2014, **2**, 9028–9034; (d) M. Zheng, D. T. Zhang, M. X. Sun, Y. P. Li, T. L. Liu, S. F. Xue and W. J. Yang, *J. Mater. Chem. C*, 2014, **2**, 1913–1920; (e) H. Li, Z. Chi, B. Xu, X. Zhang, X. Li, S. Liu, Y. Zhang and J. Xu, *J. Mater. Chem.*, 2011, **21**, 3760–3767; (f) W. Liu, Y. Wang, M. Sun, D. Zhang, M. Zheng and W. Yang, *Chem. Commun.*, 2013, **49**, 6042–6044; (g) X. Zhang, Z. Chi, X. Zhou, S. Liu, Y. Zhang and J. Xu, *J. Phys. Chem. C*, 2012, **116**, 23629−23638; (h) Y. Dong, B. Xu, J. Zhang, X. Tan, L. Wang, J. Chen, H. Lv, S. Wen, B. Li, L. Ye, B. Zou and W. Tian, *Angew. Chem. Int. Ed.*, 2012, **51**, 10782–10785; (i) H. Li, X. Zhang, Z. Chi, B. Xu, W. Zhou, S. Liu, Y. Zhang and J. Xu, *Org. Lett.*, 2011, **13**, 556–559; (j) Q. Qi, Y. Liu, X. Fang, Y. Zhang, P. Chen, Y. Wang, B. Yang, B. Xu, W. Tian and S. X.-A. Zhang, *RSC Adv.*, 2013, **3**, 7996–8002.

13 (a) Y. Cao, W. Xi, L. Wang, H. Wang, L. Kong, H. Zhou, J. Wu and Y. Tian, *RSC Adv.*, 2014, **4**, 24649–24652; (b) J. Sun, Y. Dai, M. Ouyang, Y. Zhang, L. Zhan and C. Zhang, *J. Mater. Chem. C*, 2015, **3**, 3356–3363; (c) Y. Zhang, K. Wang, G. Zhuang, Z. Xie, C. Zhang, F. Cao, G. Pan, H. Chen, B. Zou and Y. Ma, *Chem. Eur. J.*, 2015, **21**, 2474–2479; (d) Z. Zhang, B. Xu, J. Su, L. Shen, Y. Xie and H. Tian, *Angew. Chem. Int. Ed.* 2011, **50**, 11654–11657.

14 Y. Hong, J. W. Y. Lam and B. Z. Tang, *Chem. Soc. Rev.*, 2011, **40**, 5361−5388.

15 (a) X. Sun, X. Zhang, X. Li, S. Liu and G. Zhang, *J. Mater. Chem.*, 2012, **22**, 17332−17339; (b) Y. Gong, Y. Tan, J. Liu, P. Lu, C. Feng, W. Yuan, Y. Lu, J. Sun, G. He and Y. Zhang, *Chem. Commun.*, **2013**, *49*, 4009−4011; (c) Y. Sagra and T. Kato, *Angew. Chem. Int. Ed.*, 2011, **50**, 9128−9132; (d) C. Dou, D. Chen, J. Iqbal, Y. Yuan, H. Zhang and Y. Wang, *Langmuir*, 2011, **27**, 6323−6329; (e) P. Xue, P. Chen, J. Jia, Q. Xu, J. Sun, B. Yao, Z. Zhang and R. Lu, *Chem. Commun.*, 2014, **50**, 2569−2571; (f) G. Zhang, J. Sun, P. Xue, Z. Zhang, P. Gong, J. Peng and R. Lu. *J. Mater. Chem. C*, 2015, **3**, 2925−2932.

16 Z. Guo, W. Zhu and H. Tian, *Chem. Commun.*, 2012, **48**, 6073−6084.

17 (a) H. Tong, M. Häussler, Y. Dong, Z. Li, B. Mi, H. S. Kwok and B. Z. Tang, *J. Chin. Chem. Soc.* (Taipei) 2006, **53**, 243−246; (b) H. Tong, Y. Dong, M. Häussler, Y. Hong, J. Lam, H. Sung, I. D. Williams, H. S. Kwok and B. Z. Tang, *Chem. Phys. Lett.*, 2006, **428**, 326−330.

18 H. Tong, Y. Hong, Y. Dong, Y. Ren, M. Häussler, J. W. Y. Lam, K. S. Wong and B. Z. Tang, *J. Phys. Chem. B*, 2007, **111**, 2000−2007.

19 (a) X. Zhang, Z. Chi, B. Xu, L. Jiang, X. Zhou, Y. Zhang, S. Liu and J. Xu, *Chem. Commun.*, 2012, **48**, 10895–10897; (b) P. Xue, B. Yao, X. Liu, J. Sun, P. Gong, Z. Zhang, C. Qian, Y. Zhang and R. Lu, *J. Mater. Chem. C*, 2015, **3**, 1018–1025; (c) P. Xue, J. Sun, P. Chen, P. Gong, B. Yao, Z. Zhang, C. Qian and R. Lu, *J. Mater. Chem. C*, 2015, **3**, 4086–4092.

20 C. Wang, G. Wang, Z. Wang and X. Zhang, *Chem. Eur. J.*, 2011, **17**, 3322–3325.

21 L. L. Woods, *J. Am. Chem. Soc*, 1958, **80**, 1440−1442.

22 H. Li, Y. Guo, G. Li, H. Xiao, Y. Lei, X. Huang, J. Chen, H. Wu, J. Ding and Y. Cheng, *J. Phys. Chem. C*, 2015, **119**, 6737–6748.

23 Y. L. Wang, T. L. Liu, L. Y. Bu, J. F. Li, C. Yang, X. J. Li, Y. Tao and W. J. Yang, *J. Phys. Chem. C*, 2012, **116**, 15576–15583.

24 (a) X. Zhang, Z. Yang, Z. Chi, M. Chen, B. Xu, C. Wang, S. Liu, Y. Zhang and J. Xu, *J. Mater. Chem.*, 2010, **20**, 292–298; (b) Y. Q. Dong, J. W. Y. Lam, A. J. Qin, J. X. Sun, J. Z. Liu, Z. Li, J. Z. Sun, H. H. Y. Sung, I. D. Williams, H. S. Kwok and B. Z. Tang, *Chem. Commun.*, 2007, 3255–3257.

25 H. Auweter, H. Haberkorn, W. Heckmann, D. Horn, E. Lüddecke, J. Rieger and H. Weiss, *Angew. Chem. Int. Ed.*, 1999, **38**, 2188−2191.

26 J. Chen, C. C. W. Law, J. W. Y. Lam, Y. Dong, S. M. F. Lo, I. D. Williams, D. Zhu and B. Z. Tang, *Chem. Mater.*, 2003, **15**, 1535−1546.

27 X. Y. Shen, Y. J. Wang, E. Zhao, W. Z. Yuan, Y. Liu, P. Lu, A. Qin, Y. Ma, J. Z. Sun and B. Z. Tang, *J. Phys. Chem. C*, 2013, **117**, 7334−7347.

Indene-1,3-dionemethylene-4*H*-pyran derivatives containing alkoxy chains of various lengths: Aggregation-induced emission enhancement, mechanofluorochromic properties and solvent-induced emission changes

Yanze Liu, Yunxiang Lei, Fei Li, Jiuxi Chen, Miaochang Liu, Xiaobo Huang, Wenxia Gao, Huayue Wu, Jinchang Ding and Yixiang Cheng

A series of D-π-A indene-1,3-dionemethylene-4*H*-pyran derivatives with aggregation-induced emission enhancement phenomena exhibit not only reversible solid-state fluorescence changes induced by external stimuli, but also alkoxy chain length-dependent fluorescence properties.